Supplementary Information

Translational T-box riboswitches bind tRNA by modulating conformational flexibility

Eduardo Campos-Chavez[1, #], Sneha Paul[2,4, #], Zunwu Zhou[2], Dulce Alonso[1], Anjali R. Verma[3,5], Jingyi Fei[2,*], and Alfonso Mondragón[1,*]

[1]Department of Molecular Biosciences, Northwestern University, Evanston, IL 60208, USA.
[2]Department of Biochemistry and Molecular Biology and Institute for Biophysical Dynamics, The University of Chicago, Chicago, IL 60637, USA.
[3]Department of Chemistry, Columbia University, New York, NY 10027, USA.

[4]Current address: Institute of Molecular Sciences of Orsay, Paris-Saclay University, 91405 Orsay, France.
[5]Current address: Biophysics Program and Institute for Physical Sciences and Technology, University of Maryland, College Park, MD 20742, USA.

[#]These authors contributed equally
*Correspondence to Jingyi Fei (jingyifei@uchicago.edu) or Alfonso Mondragón (a-mondragon@northwestern.edu)

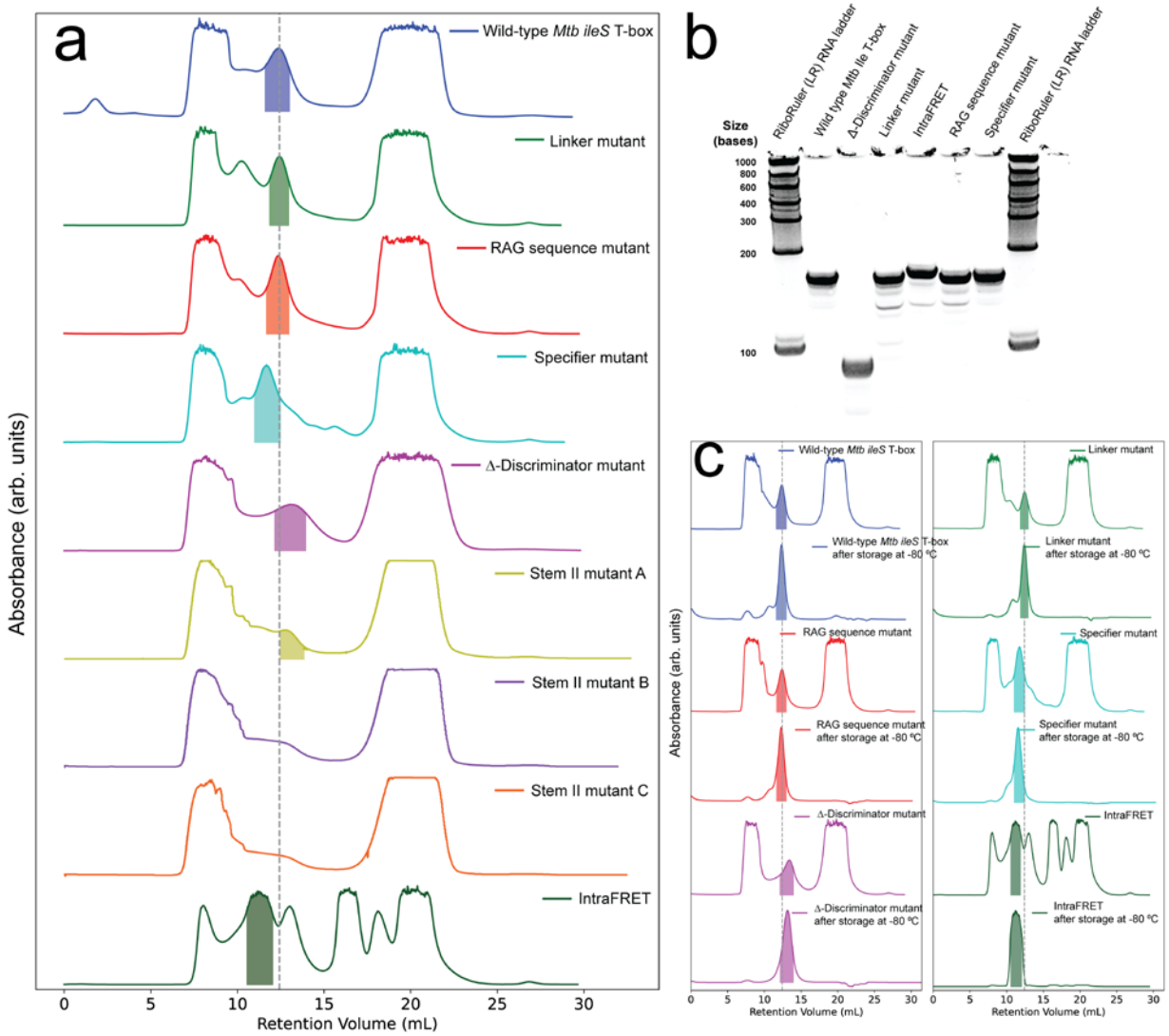

Supplementary Figure S1. *Mtb-ileS* T-box riboswitch purification. a) Size exclusion chromatography (SEC) elution profiles of the different constructs. The shaded regions correspond to the fractions that were selected for the FRET and BLI experiments. Slight variation in the elution of the T-box probably corresponds to changes in the hydrodynamic radius of the molecule. For Stem II Mutant B and C (**Supplementary Fig. S7**), there was no clear peak detected, probably indicating that these mutants were misfolded. The T-box construct for intramolecular FRET measurement, with two dyes attached, elutes more rapidly reflecting the larger size of this molecule. **b)** Denaturing gel of the construct characterized by smFRET. After purification, the samples were stored at -80 ºC for later use. The gel was run using samples stored for 1 week and shows that there is no degradation of the samples after storage. Samples are identified on top of the gel. Molecular weight markers are shown on the rightmost and leftmost lanes. **c)** SEC profiles of the samples right after purification (left) and one week after purification and storage at -80 ºC. The rightmost elution profiles show that the samples stay intact and folded after storage.

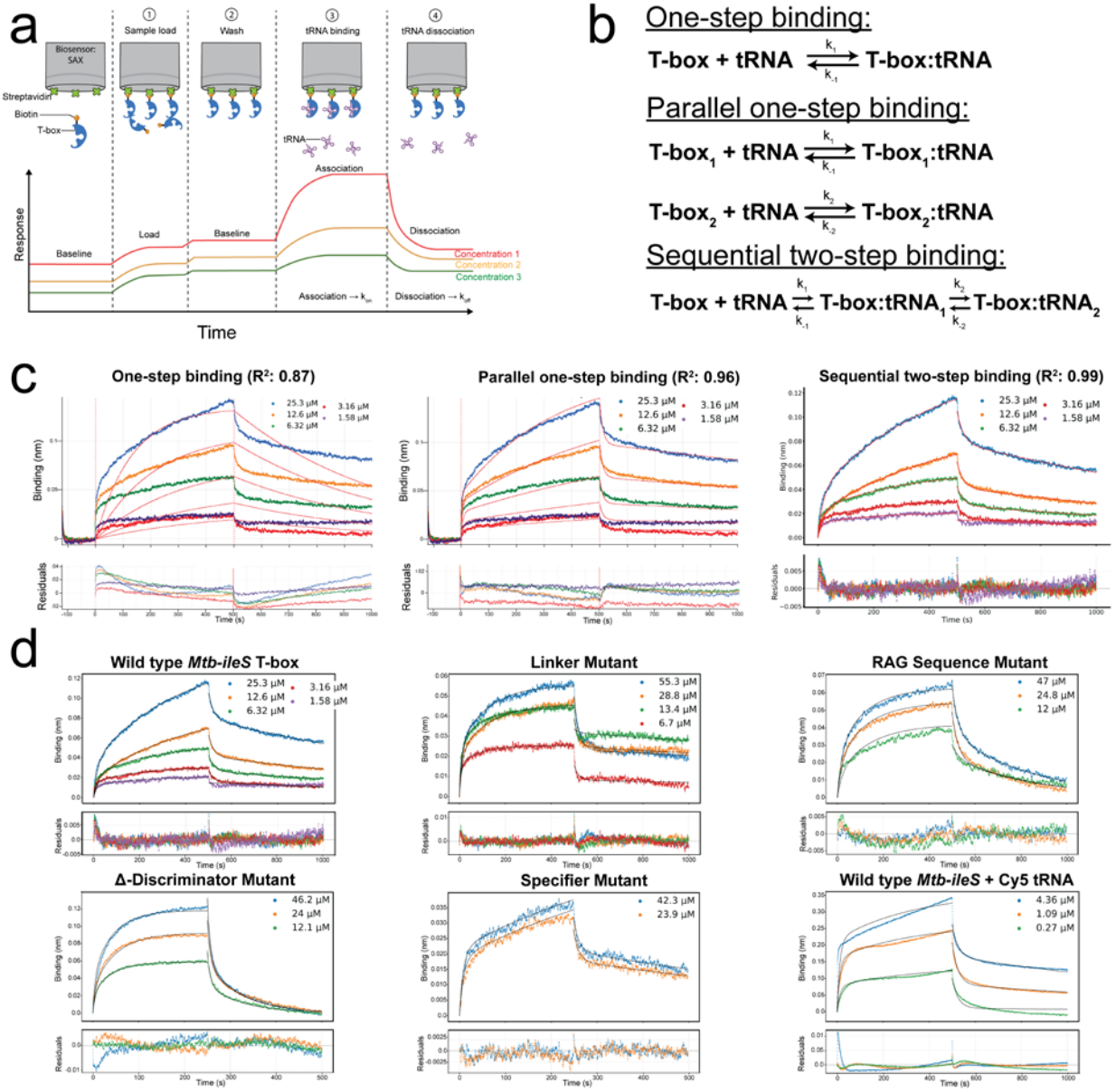

Supplementary Figure S2. BLI analyses of the *Mtb-ileS* T-box riboswitch binding. a) Schematic diagram showing the steps in the BLI experiment. In general, the experiment consists of four steps: loading of the labeled T-box, wash, binding of the tRNA (association step), and wash with buffer (dissociation step). During these steps, the response is measured against time. For analysis, only the last two steps, association and dissociation, are considered. **b)** Kinetic models considered to describe the BLI binding process: a one-step binding mechanism where the T-box and the tRNA bind in one single step, a parallel one-step binding scheme, where the two binding sites (anticodon:specifier and NCCA:T-box sequence) bind simultaneously but independently, and a sequential two-step binding scheme. **c)** BLI data on tRNA association and dissociation for the wild-type *Mtb-ileS* T-box was fit to the three kinetic models: one-step binding, parallel one-step binding, and sequential two-step binding. The sequential two step-binding model best fits the data (R^2 = 0.99) compared to the other models. The fits are shown by an orange dashed or solid line. The fit residuals are shown at the bottom. **d)** Fit of the BLI data for different

constructs. In all cases, the sequential two-step binding model was used. The different tRNA concentrations used are shown by different colors and the concentrations are shown next to the plot. The fit is shown by a black solid line. The fit residuals are shown at the bottom. In some cases, like the specifier mutant, the binding was too weak to measure accurately more than a few concentrations. Descriptions of the binding model and the fitting procedure are found in the **Supplementary Methods** section. The fitting parameters are reported in **Supplementary Table 1**.

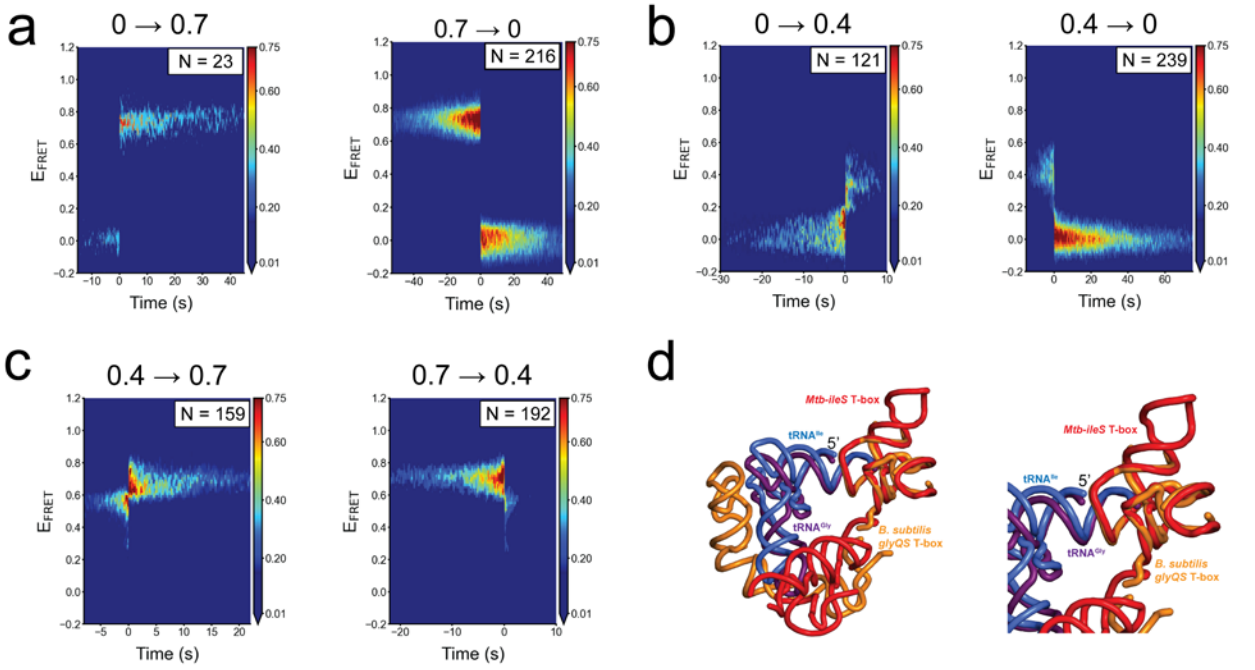

Supplementary Figure S3. smFRET experiments of tRNA^{Ile} binding to the wild-type *Mtb-ileS* T-box riboswitch show two distinct states. a) Contour plots of the time-evolved FRET efficiency histogram displaying the transitions from the zero to 0.7 FRET state (left), and from 0.7 to zero FRET state (right). The data are synchronized with t = 0 corresponding to the transition point. N reports the number of transitions in each plot. The plots are contoured using normalized counts from 0.0 (blue) to 0.75 (red). **b)** Contour plots of the time-evolved FRET efficiency histogram displaying the transitions from the zero to 0.4 FRET state (left), and from 0.4 to zero FRET state (right). **c**) Contour plots of the time-evolved FRET efficiency histogram displaying the transitions from 0.4 to 0.7 FRET state (left), and from 0.7 to 0.4 FRET state (right). **d)** Superposition of the structure of *B. subtilis glyQS* T-box riboswitch/tRNA^{Gly} complex (orange, purple) [1] on the *Mtb-ileS* T-box riboswitch/tRNA^{ile} complex (red, blue) [2]. The discriminator domains in the two structures were superposed to emphasize their similarity. The cartoon on the left shows the superposition of the two complexes, while the cartoon on the right shows a zoom of the discriminator domains. Overall, the superposition shows the high structural conservation of the discriminator domains and the way it interacts with the 3' end of the tRNA.

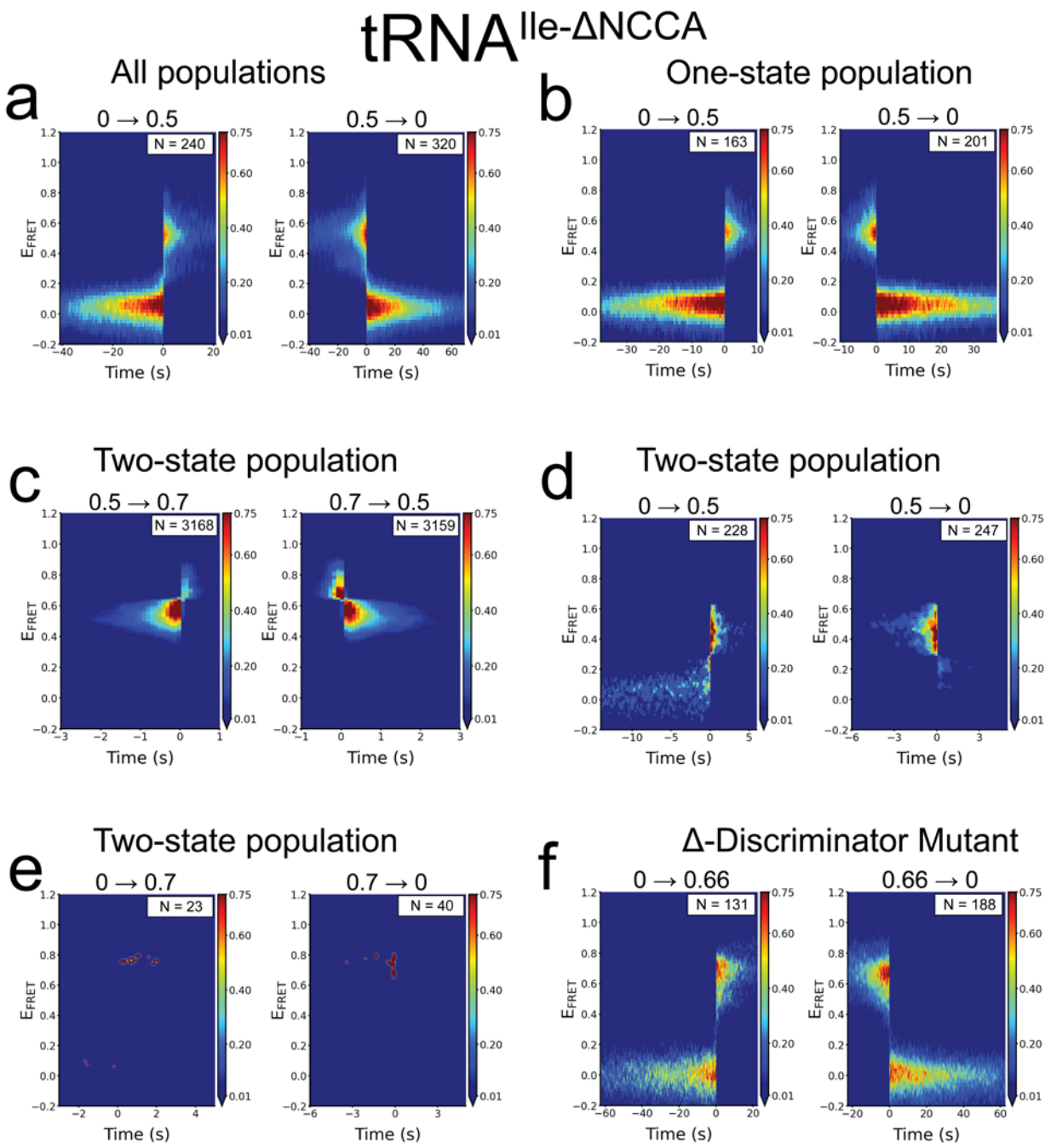

Supplementary Figure S4. smFRET experiments with mutants defective in discriminator binding help identify intermediate step. a) Contour plots of the time-evolved FRET efficiency histogram displaying transitions from the zero to 0.5 FRET state (left), and from 0.5 to zero FRET state (right) for all populations of the *Mtb-ileS* T-box riboswitch/ $tRNA^{Ile\text{-}\Delta NCCA}$-Cy5 complex. The data are synchronized with t = 0 corresponding to the transition point. N reports the number of transitions in each plot. The plots are contoured using normalized counts from 0.0 (blue) to 0.75 (red). **b)** Contour plots of a time-evolved FRET efficiency histogram displaying transitions from the zero to 0.5 FRET state (left), and from 0.5 to zero FRET state (right) for the One-state subpopulation of the *Mtb-ileS* T-box riboswitch/ $tRNA^{Ile\text{-}\Delta NCCA}$-Cy5 complex. **c)** Contour plots of a

time-evolved FRET efficiency histogram displaying transitions from the 0.5 to 0.7 FRET state (left), and from 0.7 to 0.5 FRET state (right) for the Two-state subpopulation of the *Mtb-ileS* T-box riboswitch/ $tRNA^{Ile\text{-}\Delta NCCA}$-Cy5 complex. **d)** Contour plots of a time-evolved FRET efficiency histogram displaying transitions from the zero to 0.5 FRET state (left), and from 0.5 to zero FRET state (right) for the Two-state subpopulation of the *Mtb-ileS* T-box riboswitch/ $tRNA^{Ile\text{-}\Delta NCCA}$-Cy5 complex. **e)** Contour plots of a time-evolved FRET efficiency histogram displaying transitions from the zero to 0.7 FRET state (left), and from 0.7 to zero FRET state (right) for the Two-state subpopulation of the *Mtb-ileS* T-box riboswitch/ $tRNA^{Ile\text{-}\Delta NCCA}$-Cy5 complex. **f)** Contour plots of a time-evolved FRET efficiency histogram of the *Mtb-ileS* T-box riboswitch Δ-Discriminator Mutant and $tRNA^{Ile}$ complex displaying transitions from zero to 0.66 FRET state (left) and 0.66 to zero FRET state (right).

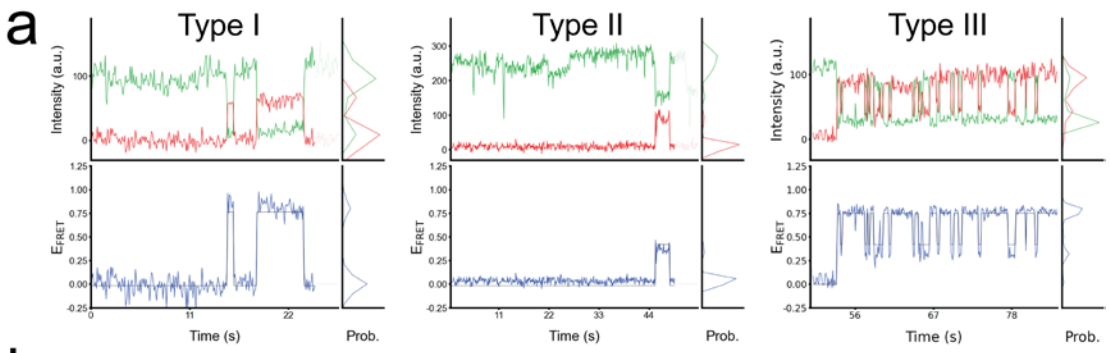
a
Type I
Type II
Type III
Intensity (a.u.)
E_FRET
Time (s)
Prob.

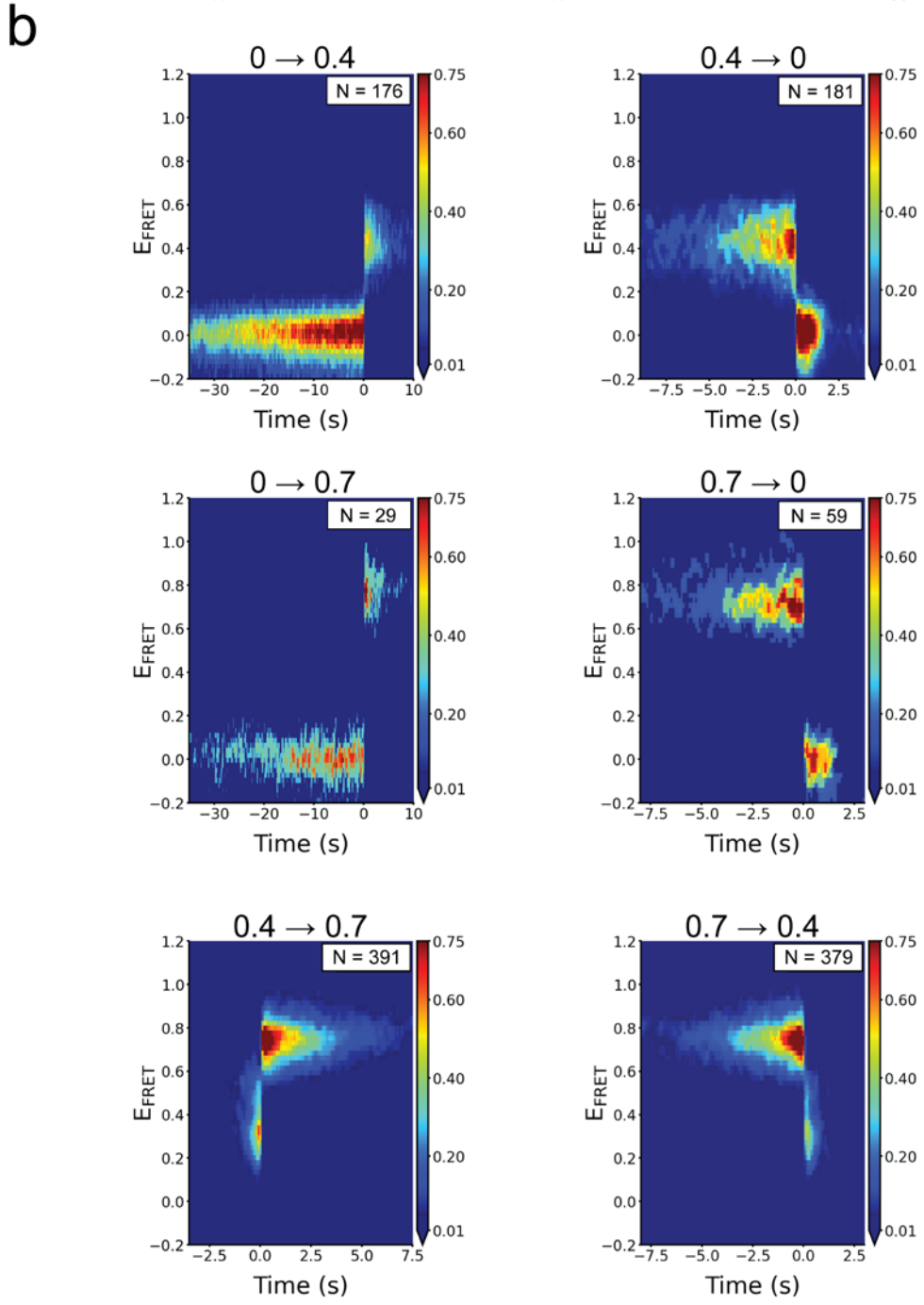
b
0 → 0.4
N = 176
0.4 → 0
N = 181
0 → 0.7
N = 29
0.7 → 0
N = 59
0.4 → 0.7
N = 391
0.7 → 0.4
N = 379
E_FRET
Time (s)

Supplementary Figure S5. smFRET experiments with Linker Mutant show the importance of regions not directly contacting the NCAA sequence. a) Representative Cy3 (green) and Cy5 (red) fluorescence intensity trajectories (top) and corresponding smFRET trajectories (bottom) for the Linker Mutant *Mtb-ileS* T-box riboswitch/tRNA^{Ile} complex for the three types of traces identified. smFRET efficiency was calculated as (I_{Cy5}/(I_{Cy3}-I_{Cy5}). **b)** Contour plots of a time-evolved FRET efficiency histogram of the Linker Mutant *Mtb-ileS* T-box riboswitch/ tRNA^{Ile} complex displaying transitions between zero and 0.4 FRET state (top), between zero and 0.7 FRET state (middle), and between 0.4 and 0.7 FRET state (bottom). The data are synchronized with t = 0 corresponding to the corresponding transition point. N reports the number of transitions in each plot. The plots are contoured using normalized counts from 0.0 (blue) to 0.75 (red).

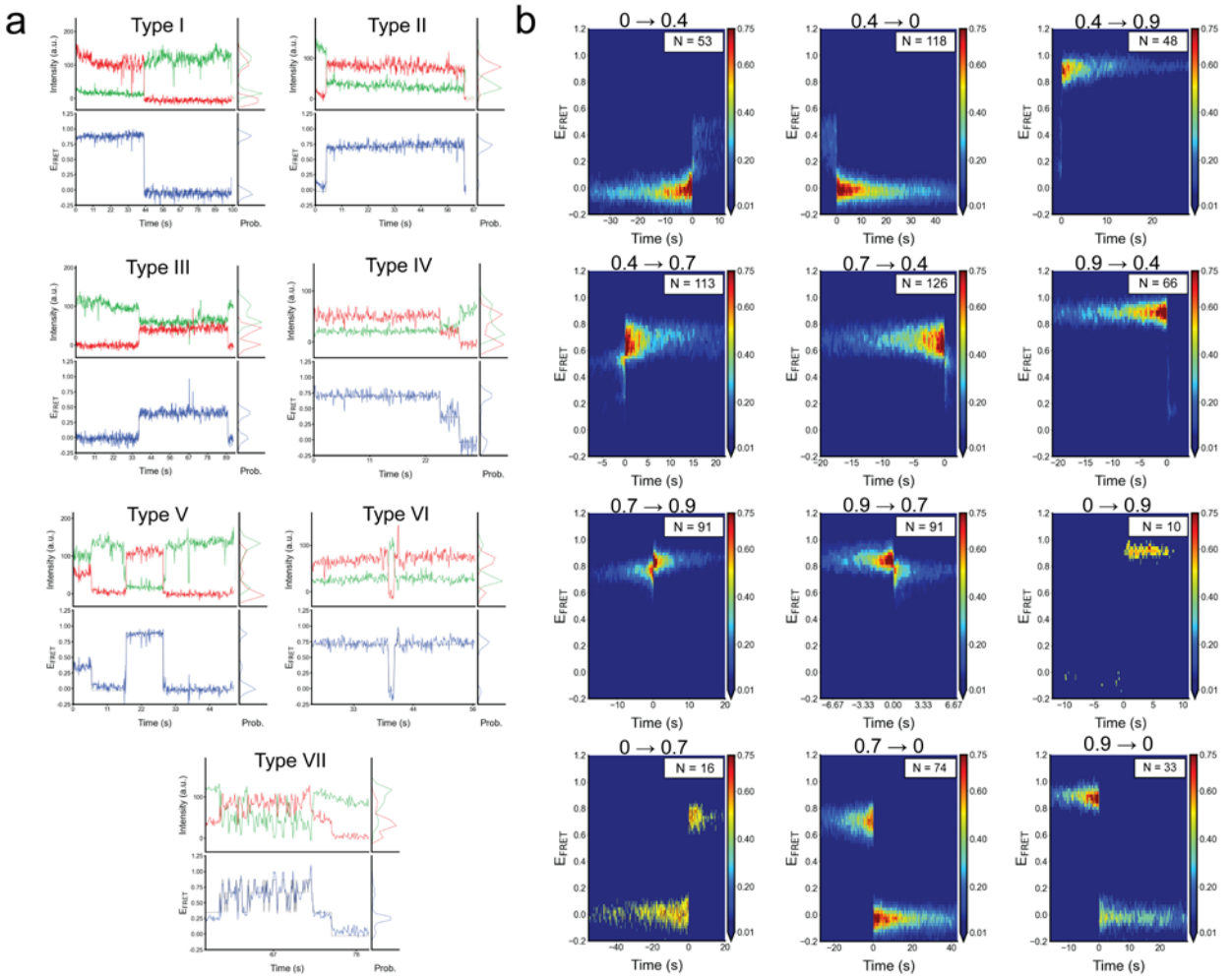

Supplementary Figure S6. smFRET experiments with RAG Sequence mutant show the importance of contacts around the NCAA sequence. a) Representative Cy3 (green) and Cy5 (red) fluorescence intensity trajectories (top) and corresponding smFRET trajectories (bottom) for the RAG Sequence mutant *Mtb-ileS* T-box riboswitch/tRNA^{Ile} complex for all the types of traces identified. smFRET efficiency was calculated as (I_{Cy5}/(I_{Cy3}-I_{Cy5}). **b)** Contour plots of time-evolved FRET efficiency histograms showing all transitions in the RAG Sequence mutant *Mtb-ileS* T-box riboswitch/ tRNA^{Ile} complex. The data are synchronized with t = 0 corresponding to the corresponding transition point. N reports the number of transitions in each plot. The plots are contoured using normalized counts from 0.0 (blue) to 0.75 (red).

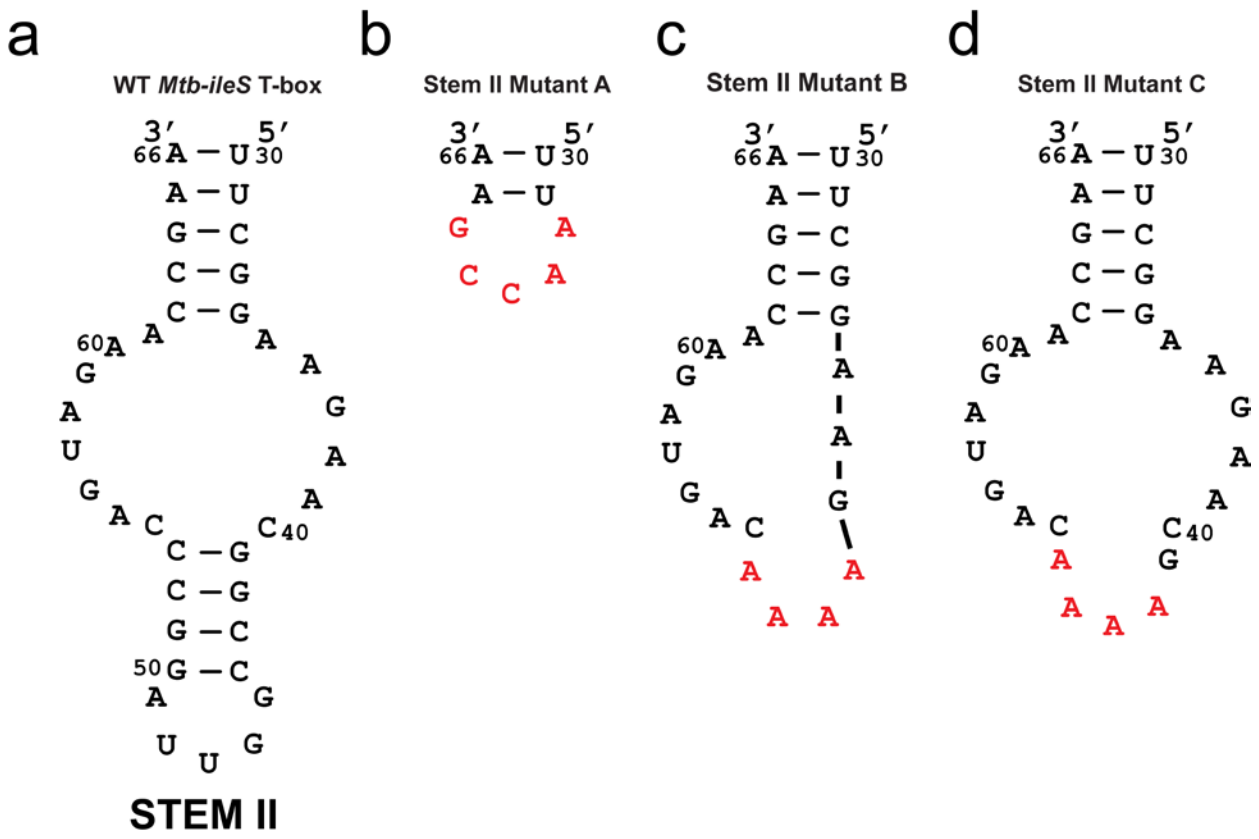

Supplementary Figure S7. *Mtb-ileS* T-box riboswitch Stem II mutants analyzed. a) Schematic diagram showing the sequence and paired regions in the wild-type Stem II in the *Mtb-ileS* T-box riboswitch. **b)** Schematic diagram of Stem II Mutant A where almost the entire Stem II (nucleotides 32-64) was deleted. **c)** Schematic diagram of Stem II Mutant B where one large region (nucleotides 38 -53), including the bottom paired region, was removed. **d)** Schematic diagram of Stem II Mutant C where the entire bottom paired region (nucleotides 42-53) was removed. In all diagrams new nucleotides introduced to form a loop are shown in red. Numbering according to the wild-type molecule.

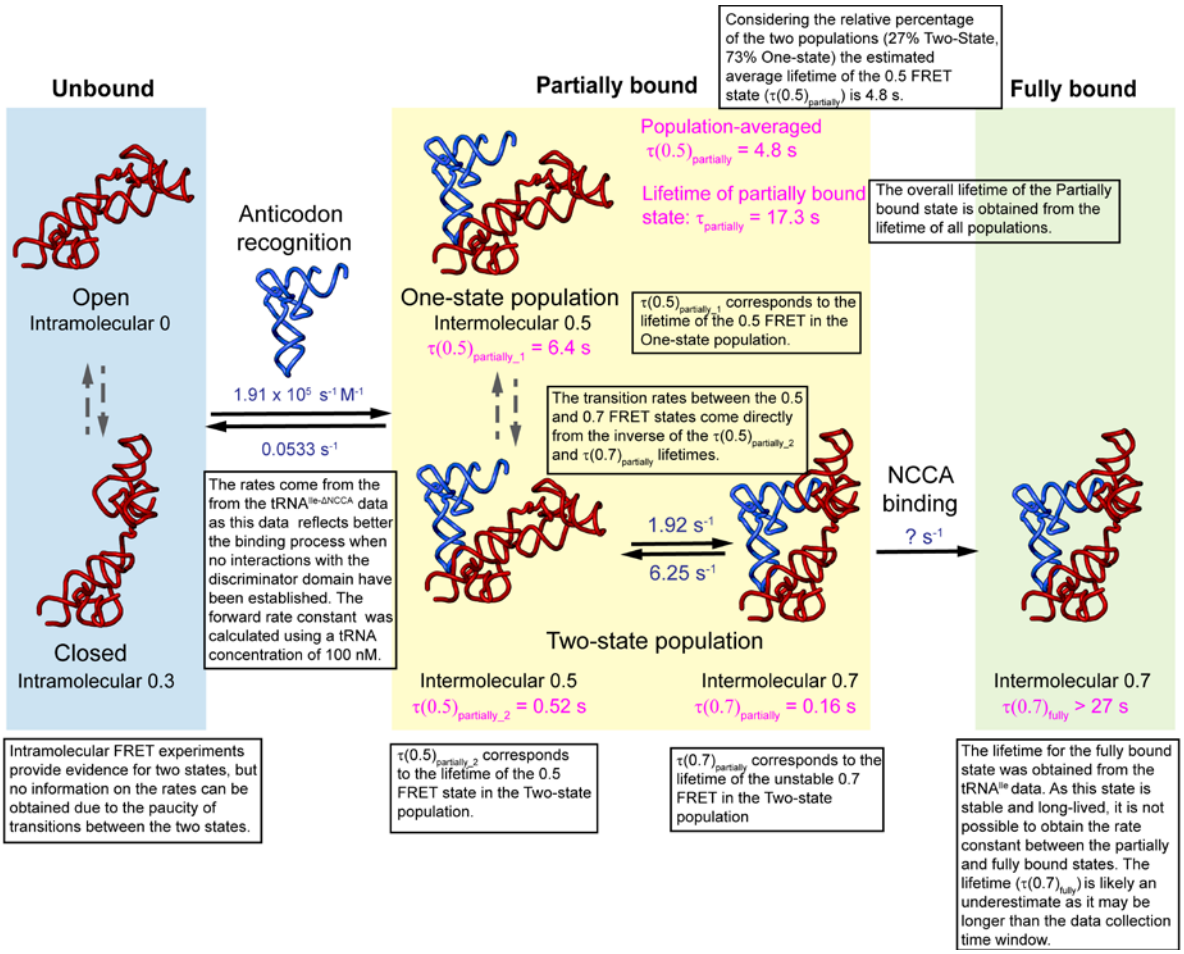

Supplementary Figure 8. Annotated version of Figure 8. The figure shows Figure 8 with annotations, that, together with the explanation below, help understand how the rates were determined. The final model is based on a combination of data from the wild-type *Mtb ileS* T-box in complex with tRNA^{Ile} and tRNA$^{Ile\text{-}\Delta NCCA}$. This combination gives a better representation of the fully and partially bound states.

A) Unbound state.

The intramolecular labeled *Mtb ileS* T-box FRET experiments provide the information on the ligand-free *Mtb ileS* Tbox. Two FRET states at zero and 0.3 were observed (**Fig. 5**), which were assigned to open and closed conformations respectively. In these experiments not many reversible transitions between the zero and 0.3 FRET were observed, suggesting that the transition rate between the open and closed conformations may be slower than the imaging time window. Therefore, it is difficult to estimate the transition rates between the 0.3 and zero FRET states, and these transitions are marked as dashed arrows with rates unknown. Since binding of tRNA shifts the equilibrium to the closed conformation (**Fig. 5**), it is most likely that the closed conformation corresponds to the tRNA bound state. However, future 3-color smFRET experiments are needed to ascertain whether tRNA binds preferentially to one state or the other.

B) Fully bound state.

The fully bound state refers to a state after anticodon and NCCA binding. The fully bound state corresponds to the 0.7 FRET state. In the presence of tRNA^{Ile}, the majority of the traces only show a stable FRET state at 0.7 (Type I-1, 71.0%, **Supplementary Table 3**), suggesting that when both the anticodon and uncharged NCCA end are present, the *Mtb ileS* T-Box/tRNA^{Ile} complex is very stable. As this stable population is already formed prior to the

start of the imaging experiment, it provides a good estimate of the overall stability of the fully bound state, but with limited kinetic information related to reaching that state. We therefore estimate the lifetime of the fully bound 0.7 FRET state from the $tRNA^{Ile}$ data. The lifetime of the fully bound 0.7 state ($\tau(0.7)_{fully}$ > 28 s) is probably an underestimate due to i) the complex already being formed when measurements start and ii) bleaching of the fluorophores.

C) Partially bound state

In the $tRNA^{Ile}$ experiments, 17.8% of the traces only sample the 0.4 FRET state (Type II, **Supplementary Table 3**), and 4.9% sample both the 0.4 and 0.7 FRET state (Type III, **Supplementary Table 3**), which represent either the population that fails to reach the stable fully bound state or a slow population in the binding process. Therefore, whereas Type II and III traces are indicative of the presence of the 0.4 FRET state, they do not represent the majority of the population and are not ideal to reveal accurately or confidently the binding rates. On the other hand, experiments using $tRNA^{Ile\text{-}\Delta NCCA}$ contain more kinetic information on the partially bound state. $tRNA^{Ile\text{-}\Delta NCCA}$ shows repetitive binding from the unbound state to the partially bound state and repetitive attempts to reach a 0.7 state from the 0.5 state within the partially bound state (**Fig. 4**). For this reason, we use the $tRNA^{Ile\text{-}\Delta NCCA}$ to determine parameters related to the first binding step and conformational sampling within the partially bound state.

(1) *Rate constants for anticodon recognition step.* Binding and dissociation rates between the unbound state and partially bound state are calculated directly from the transition matrix through Global HMM modeling (**Supplementary Table 5**) using $tRNA^{Ile\text{-}\Delta NCCA}$. The binding rate constant is calculated using a tRNA concentration of 100 nM.

(2) *Rate constants for conformation sampling in the partially bound state.* $tRNA^{Ile\text{-}\Delta NCCA}$ transiently samples the 0.7 FRET state, but without establishing a stable interaction with the discriminator domain due to the absence of the NCCA sequence to base pair with the T-box sequence. Thus, the $tRNA^{Ile\text{-}\Delta NCCA}$ data also provide kinetic information for the conformational sampling step before the formation of the stable fully bound state. This conformational sampling of the 0.7 FRET state is observed within the Two-state subpopulation of the partially bound state. The lifetime of the 0.5 FRET ($\tau(0.5)_{partially\_2}$) and 0.7 FRET ($\tau(0.7)_{partially}$) within the Two-state subpopulation are determined by dwell time analysis using Composite HMM modeling (**Supplementary Table 6**). The inter-transition rates are determined using the reciprocal of the lifetimes of the initial FRET states respectively. However, since the data with $tRNA^{Ile}$ mostly report the features of an already formed complex, without capturing the actual transition to form it, we do not know how many attempts the $tRNA^{Ile}$ samples the 0.7 FRET state before securing the interaction. For this reason, we leave an unknown ("?") the rate constant for the NCCA binding step after the conformational sampling in the partially bound state.

(3) *Lifetime of the partially bound state.* In the $tRNA^{Ile\text{-}\Delta NCCA}$ experiments, the One-state population visits the 0.5 FRET state transiently from the zero state (**Fig. 4a**), whereas the Two-state population largely remains in the 0.5 FRET state but rapidly samples the 0.7 FRET state (**Fig. 4e**). $\tau(0.5)_{partially\_1}$ and $\tau(0.5)_{partially\_2}$ correspond to the lifetime of the 0.5 FRET in the One-state population and Two-state population of the partially bound state respectively. Considering the relative percentage of these two populations (27% Two-State, 73% One-state, **Supplementary Table 3**), the average lifetime of the 0.5 FRET state ($\tau(0.5)_{partially}$) is estimated to be 4.8 s. $\tau(0.7)_{partially}$ corresponds to the lifetime of the unstable 0.7 FRET state in the Two-state population. The overall lifetime of the Partially bound state ($\tau_{partially}$ = 17.3 s) is obtained from the lifetime of all populations in the $tRNA^{Ile\text{-}\Delta NCCA}$ data (**Supplementary Table 4**).

D) Consistency between rates calculated from the $tRNA^{Ile}$ and $tRNA^{Ile\text{-}\Delta NCCA}$ data

(1) *Binding rate constant of anticodon recognition step.* Assuming the zero to 0.4 FRET and zero to 0.7 FRET transitions in the Type I-2, Type II, and Type III traces report the binding

rate of WT $tRNA^{Ile}$ (Type I-1 traces are stable at 0.7 and do not transition from zero), the transition rate from zero to any non-zero state is 0.0094 s^{-1} at 100 nM $tRNA^{Ile}$ (**Supplementary Table 5**), which is 51% slower than the transition rate from zero to 0.5 FRET at 100 nM $tRNA^{Ile\text{-}\Delta NCCA}$ (0.019 s^{-1}, **Supplementary Table 5**).

(2) *Transitions from the 0.4 state.* The transition rate out of the 0.4 FRET state to any other FRET state (zero or 0.7 FRET) is 0.144 s^{-1} in the presence of $tRNA^{Ile}$ (**Supplementary Table 5**), whereas the transition out of 0.5 FRET to zero (dissociate) or 0.7 (attempt to sample the 0.7 FRET state) is 0.21 s^{-1} in the presence of $tRNA^{Ile\text{-}\Delta NCCA}$, the former being 31% slower than the latter rate.

These consistencies support the notion that the minor populations observed in $tRNA^{Ile}$ data that have not reached the stable 0.7 FRET represent a population that either fails to reach the stable full bound state or is a slow population in the kinetic process.

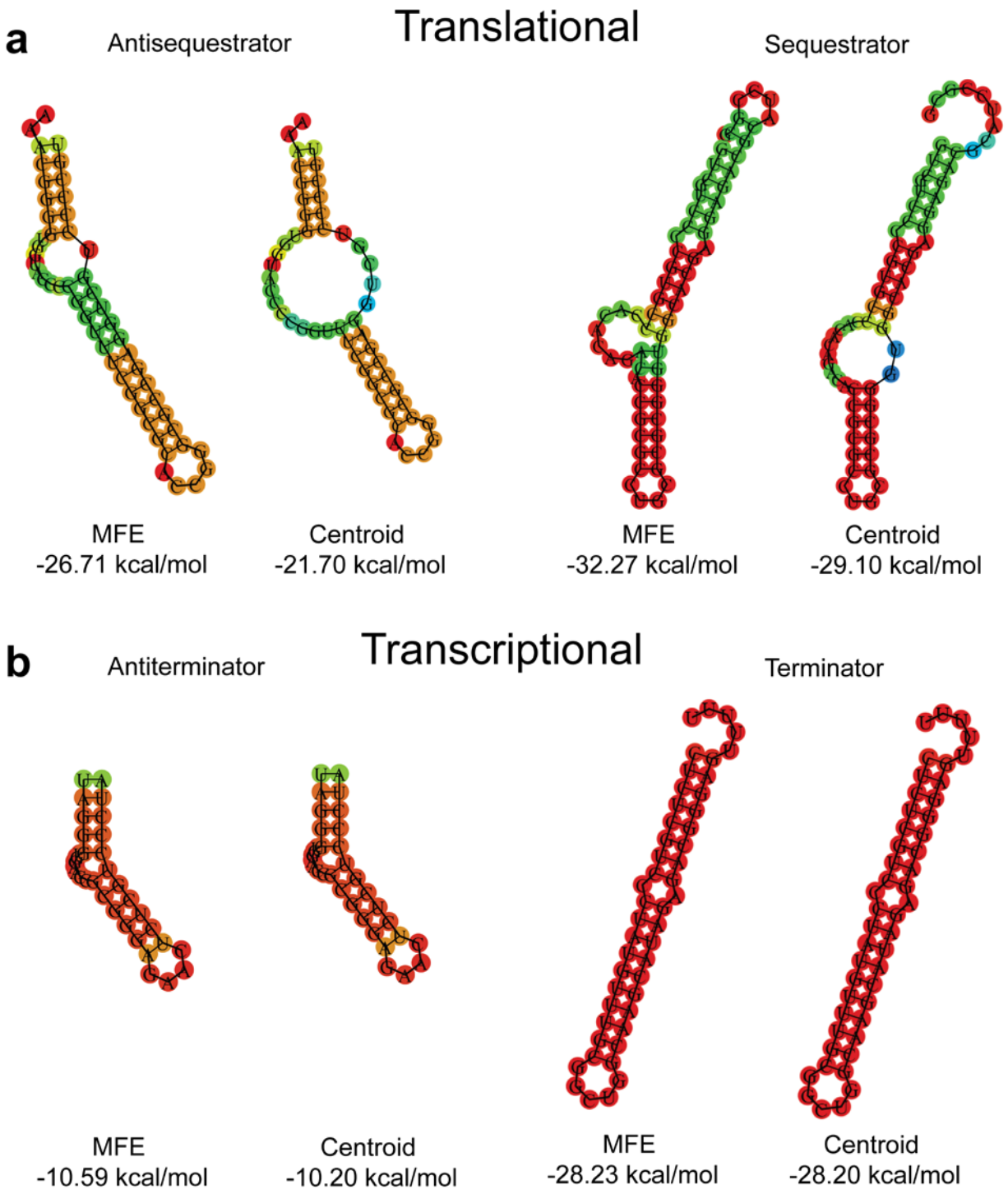

Supplementary Figure 9. Potential structures of the terminator/antiterminator and sequestrator/antisequestrator sequences predicted using the RNAfold web server [3]. a) Predicted structures for the *Mtb IleS* T-box riboswitch. **b)** Predicted structures for the *B. subtilis glyQS* T-box riboswitch. The predicted Minimum Free Energy (MFE) secondary structure and centroid structure are shown for each configuration. The MFE and centroid energy associated with each predicted structure is listed below the diagram.

Biolayer interferometry (BLI) parameters fit to a two-step sequential model							
	k_1 ($M^{-1} \cdot s^{-1}$)	k_{-1} (s^{-1})	k_2 (s^{-1})	k_{-2} (s^{-1})	K_D (μM)	R^2 dissociation	R^2 association
Wild type *Mtb Ile* T-box + Unlabeled tRNA	9204.86 ± 458.05	0.0365 ± 0.0005	0.0079 ± 0.0001	0.0009 ± 0.000005	0.42 ± .022	0.996	0.997
Wild type *Mtb Ile* T-box + Cy5 tRNA	6178.69 ± 2150.44	0.0351 ± 0.0003	0.0041 ± 0.00004	0.0008 ± 0.000006	0.89 ± 0.31	0.985	0.980
Linker Mutant	4998.83 ± 18.29	0.0335 ± 0.0033	0.0152 ± 0.0004	0.0004 ± 0.00005	0.17 ± 0.042	0.975	0.989
RAG Mutant	10138 ± 1403.78	0.0460 ± 0.0031	0.0242 ± 0.0024	0.0088 ± 0.0005	1.2 ± 0.21	0.984	0.984
Specifier Mutant	160.12 ± 4.33	0.0871 ± 0.0017	0.0048 ± 0.000003	0.0014 ± 0.00002	120.4 ± 4.23	0.916	0.973
Δ-Discriminator Mutant	9727.35 ± 1154.80	0.1179 ± 0.0079	0.0347 ± 0.0070	0.0173 ± 0.0012	4.03 ± 0.80	0.991	0.993

Supplementary Table 1. Parameters fitted to the BLI data. The table shows the fitting parameters and R^2 residual for tRNA association and dissociation for each construct. The sequential two-step binding model was used to fit the BLI data. The fit and the error estimates were calculated as described in the **Methods** and **Supplementary Methods** section. A diagram showing the fit to the data for the different constructs is shown in **Supplementary Fig. S2.**

Sample	Mean	Variance	Fraction
Wild-type *Mtb-ileS* T-box + tRNA^{Ile}			
State 1	-0.0081	0.0095	0.5901
State 2	0.4212	0.0165	0.0990
State 3	0.7357	0.0087	0.3110
Wild-type *Mtb-ileS* T-box + tRNA$^{Ile\text{-}\Delta NCCA}$			
Two-State			
State 1	0.0368	0.0104	0.2426
State 2	0.5235	0.0067	0.4941
State 3	0.6951	0.0120	0.2634
One-state			
State 1	0.0318	0.0060	0.8941
State 2	0.5332	0.0144	0.1059
General			
State 1	0.0284	0.0107	0.7010
State 2	0.5289	0.0260	0.2990
***Mtb-ileS* T-box Δ-Discriminator Mutant + tRNA^{Ile}**			
State 1	-0.0147	0.0150	0.7543
State 2	0.6674	0.0161	0.2457
***Mtb-ileS* T-box Linker mutant + tRNA^{Ile}**			
State 1	-0.0179	0.0115	0.7107
State 2	0.4093	0.0160	0.1181
State 3	0.7572	0.0139	0.1712
***Mtb-ileS* T-box RAG mutant + tRNA^{Ile}**			
State 1	-0.0291	0.0053	0.5667
State 2	0.3609	0.0235	0.1075
State 3	0.6950	0.0068	0.1882
State 4	0.8799	0.0045	0.1377

Supplementary Table 2. Parameters of the consensus HMM model fitted to the FRET histogram for the different constructs.

Sample	Trace type	Number	Fraction
Wild-type *Mtb-ileS* T-box + tRNA^{ile}			
	I	269	0.7730
	II	62	0.1782
	III	17	0.0488
Total		348	1.0
Type I subtypes	I-1	247	0.9182
	I-2	22	0.0818
Total		269	1.0
Wild-type *Mtb-ileS* T-box + tRNA$^{ile\text{-}\Delta NCCA}$			
	Two-state	72	0.2727
	One-state	192	0.7273
Total		264	1.0
***Mtb-ileS* T-box Δ-Discriminator Mutant + tRNA^{Ile}**			
	All	161	1.0
Total		161	1.0
***Mtb-ileS* T-box Linker mutant + tRNA^{Ile}**			
	I	40	0.2030
	II	91	0.4620
	III	66	0.3350
Total		197	1.0
Type I subtypes	I-1	8	0.2
	I-2	32	0.8
Total		40	1.0
***Mtb-ileS* T-box RAG mutant + tRNA^{Ile}**			
	I	72	0.3654
	II	35	0.1776
	III	17	0.0862
	IV	55	0.2791
	V	4	0.0203
	VI	8	0.0406
	VII	6	0.0304
Total		197	1.0

Supplementary Table 3. Categorization of smFRET trace types. The table shows the trace number and fraction of each trace type for different constructs. Refer to the text for a detailed description.

Sample	Transition	Number of events	Fraction of events
Wild-type *Mtb-ileS* T-box + tRNA^{Ile}			
	0 → 0.7	23	0.0243
	0 → 0.4	121	0.1273
	0.4 → 0	239	0.2516
	0.4 → 0.7	159	0.1674
	0.7 → 0	216	0.2273
	0.7 → 0.4	192	0.2021
Total		950	1.0
Wild-type *Mtb-ileS* T-box + tRNA$^{Ile\text{-}\Delta NCCA}$			
Two-state	0 → 0.5	228	0.0332
	0 → 0.7	23	0.0033
	0.5 → 0	247	0.0360
	0.5 → 0.7	3168	0.4615
	0.7 → 0	40	0.0058
	0.7 → 0.5	3159	0.4602
Total		6865	1.0
One-state	0 → 0.5	163	0.4478
	0.5 → 0	201	0.5522
Total		364	1.0
All populations	0 → 0.5	240	0.4286
	0.5 → 0	320	0.5714
Total		560	1.0
***Mtb-ileS* T-box Δ-Discriminator Mutant + tRNA^{Ile}**			
	0 →0.66	131	0.4106
	0.66 → 0	188	0.5894
Total		319	1.0
***Mtb-ileS* T-box Linker mutant + tRNA^{Ile}**			
	0 → 0.7	29	0.0240
	0 → 0.4	176	0.1450
	0.4 → 0	181	0.1490
	0.4 → 0.7	391	0.3220
	0.7 → 0	59	0.0486
	0.7 → 0.4	379	0.3120
Total		1215	1.0
***Mtb-ileS* T-box RAG mutant + tRNA^{Ile}**			
	0 → 0.4	53	0.0635
	0 → 0.7	16	0.0196
	0 → 0.9	10	0.0119
	0.4 → 0	118	0.1409
	0.4 → 0.7	113	0.1351
	0.4 → 0.9	48	0.0577
	0.7 → 0	74	0.0878
	0.7 → 0.4	126	0.1501
	0.7 → 0.9	91	0.1086
	0.9 → 0	33	0.0393
	0.9 → 0.4	66	0.0785
	0.9 → 0.7	91	0.1086
Total		839	1.0

Supplementary Table 4. Number of transition events identified in different smFRET experiments. The table shows the number of transitions identified and corresponding fraction in each experiment. Refer to the text for a detailed description.

Sample	Transition rate matrix					
Wild-type *Mtb-ileS* T-box + tRNA^{Ile}		Final State				
	Initial State		**0.0**	**0.4**	**0.7**	**Lifetime (s)**
		0.0	-	0.00741±0.00064	0.00195±0.00033	106.84 ± 8.22
		0.4	0.08036±0.00517	-	0.06327±0.00459	6.96 ± 0.36
		0.7	0.02367±0.00158	0.02380±0.00158	-	21.07±0.99
Wild-type *Mtb-ileS* T-box + tRNA$^{Ile-\Delta NCCA}$		Final State				
	Initial State		**0.0**	**0.5**		**Lifetime (s)**
		0.0	-	0.01905±0.00115		52.49 ± 3.17
		0.5	0.05326±0.00294	-		18.78 ± 1.04
***Mtb-ileS* T-box Δ-Discriminator Mutant + tRNA^{Ile}**		Final State				
	Initial State		**0.0**	**0.66**		**Lifetime (s)**
		0.0	-	0.01499±0.00121		66.71 ± 5.38
		0.66	0.06436 ±0.00456	-		15.53 ± 1. 1
***Mtb-ileS* T-box Linker mutant + tRNA^{Ile}**		Final State				
	Initial State		**0.0**	**0.4**	**0.7**	**Lifetime (s)**
		0.0	-	0.03326±0.0024	0.00294±0.0007	27.62 ± 1.91
		0.4	0.20843±0.0145	-	0.52650±0.0232	1.36 ± 0.05
		0.7	0.02478±0.00414	0.36332±0.016	-	2.58 ± 0.1
***Mtb-ileS* T-box RAG mutant + tRNA^{Ile}**		Final State				
	Initial State		**0.0**	**0.4**	**0.7**	**0.9**	**Lifetime (s)**
		0.0	-	0.01272±0.00136	0.00214±0.00056	0.00127±0.00043	62.0 ± 5.89
		0.4	0.12160±0.0097	-	0.10789±0.0092	0.03942±0.0055	3.72 ± 0.20
		0.7	0.02947±0.0036	0.06497 ±0.00535	-	0.06125±0.0052	7.0 ± 0.41
		0.9	0.02065±0.00348	0.04484±0.00513	0.07729 ±0.0067	-	6.42 ± 0.38

Supplementary Table 5. Transition rate matrices calculated by the consensus HMM modeling for different constructs. The units of all the rates are s^{-1}. **"**±" shows upper and lower bounds of estimated rates from the transition matrix (**Methods**). The rightmost column shows the lifetime of each initial state before transitioning into any other final state, calculated as the inverse of the sum of the transition rates out of that initial state. The lifetimes of the non-zero states are highly consistent with the lifetimes determined by dwell time analysis (**Supplementary Table 6**). Refer to the text for a description of the calculations.

Wild-type *Mtb-ileS* T-box + tRNA^{Ile}									**Lifetime**
Single exponential									
State	A	A error	k	k error					
0	0.598441	0.003901	0.050049	$4.63X10^{-4}$					
0.4	0.615317	0.005041	0.098323	0.001145					
0.7	**0.846719**	**0.002162**	**0.037198**	**1.35X10-4**					**26.88 ± 0.10**
Double exponential									
State	A_1	A_1 error	A_2	A_2 error	k_1	k_1 error	k_2	k_2 error	
0	**0.508591**	**0.004373**	**0.458205**	**0.001441**	**0.042486**	**$1.58x10^{-2}$**	**0.939521**	**$1.43x10^{-4}$**	**12.89 ± 4.6**
0.4	**0.482827**	**0.006866**	**0.416155**	**0.003407**	**0.076744**	**$3.38x10^{-2}$**	**1.0754**	**$5.83x10^{-4}$**	**7.43 ± 3.1**
Wild-type *Mtb-ileS* T-box + tRNA$^{Ile-\Delta NCCA}$ - All populations									**Lifetime**
Single exponential									
State	A	A error	k	k error					
0	**0.92386**	**0.001769**	**0.035921**	**$9.78X10^{-5}$**					**27.84 ± 0.08**
0.5	0.658982	0.005797	0.043567	$5.43X10^{-4}$					
Double exponential									
State	A_1	A_1 error	A_2	A_2 error	k_1	k_1 error	k_2	k_2 error	
0.5	**0.396166**	**0.0027**	**0.590111**	**0.001804**	**0.026613**	**$2.42X10^{-3}$**	**0.266001**	**$1.19x10^{-4}$**	**17.34 ± 1.37**
Wild-type *Mtb-ileS* T-box + tRNA$^{Ile-\Delta NCCA}$ - One state population									**Lifetime**
Single exponential									
State	A	A error	k	k error					
0	**1.016278**	**0.002224**	**0.033659**	**$1.05x10^{-4}$**					**29.71 ± 0.09**
0.5	**0.923203**	**0.004151**	**0.155983**	**$1.00X10^{-3}$**					**6.41 ± 0.04**
Wild-type *Mtb-ileS* T-box + tRNA$^{Ile-\Delta NCCA}$ - Two state population									**Lifetime**
Single exponential									
State	A	A error	k	k error					
0	0.155864	0.00387	0.048267	$1.70X10^{-3}$					
0.5	**0.884755**	**0.015595**	**1.91603**	**0.052407**					**0.52 ± 0.01**
0.7	**0.978854**	**0.012533**	**6.234466**	**$1.50x10^{-1}$**					**0.16 ± 0.004**
Double exponential									
State	A_1	A_1 error	A_2	A_2 error	k_1	k_1 error	k_2	k_2 error	
0	**0.126886**	**0.001073**	**0.857347**	**0.00848418**	**0.037456**	**$4.44X10^{-4}$**	**10.37592**	**$2.32x10^{-1}$**	**3.53 ± 0.06**
***Mtb-ileS* T-box Δ-Discriminator Mutant + tRNA^{Ile}**									**Lifetime**
Single exponential									
State	A	A error	k	k error					
0	**0.795712**	**0.002465**	**0.023707**	**$1.06x10^{-4}$**					**42.18 ± 0.19**
0.66	**0.864737**	**0.002828**	**0.062222**	**$2.89x10^{-4}$**					**16.07 ± 0.07**
***Mtb-ileS* T-box Linker mutant + tRNA^{Ile}**									**Lifetime**
Single exponential									
State	A	A error	k	k error					
0	**0.848626**	**0.013581**	**0.028197**	**6.43X10-5**					**35.46 ± 0.08**
0.4	**0.791023**	**0.015456**	**0.783887**	**0.022516**					**1.28 ± 0.04**
0.7	**0.936517**	**0.005107**	**0.338584**	**$2.66X10^{-3}$**					**2.95 ± 0.02**
***Mtb-ileS* T-box RAG mutant + tRNA^{Ile}**									**Lifetime**
Single exponential									
State	A	A error	k	k error					
0	0.680581	0.003703	0.037519	$2.92X10^{-4}$					

0.4	0.398464	0.008144	0.133559	0.003886					
0.7	**0.752927**	**0.005606**	**0.102619**	**0.001086**					**9.74 ± 0.10**
0.9	**0.827401**	**0.007053**	**0.113235**	**1.37X10^{-3}**					**8.83 ± 0.11**
Double exponential									
State	A_1	A_1 error	A_2	A_2 error	k_1	k_1 error	k_2	k_2 error	
0	**0.604831**	**0.002606**	**0.360575**	**0.007187**	**0.033329**	**1.70X10^{-4}**	**0.655285**	**2.32 x10^{-2}**	**19.37 ± 0.17**
0.4	**0.265934**	**0.007987**	**0.638568**	**0.002368**	**0.084484**	**5.65x10^{-2}**	**2.506575**	**9.35x10^{-4}**	**3.76 ± 2.33**

Supplementary Table 6. Lifetimes for the states observed for the different constructs determined by dwell time analysis. The histogram of dwell time spent on each state before transitioning out to any other state(s) is fit with either a single-exponential ($Ae^{(-tk)}$) or a double exponential decay ($A_1e^{(-tk_1)} + A_2e^{(-tk_2)}$) function. For single-exponential decay fitting, the lifetime is calculated as 1/k. For double-exponential decay fitting, the lifetime is calculated as $\frac{A_1}{A_{1+}A_2}\frac{1}{k_1} + \frac{A_2}{A_{1+}A_2}\frac{1}{k_2}$. The normalized amplitude, A, reflects the percentage of the population captured by the fitting. In other words, a small A value in a single-exponential decay fitting suggests that the fitting fails to describe the major population. In most of the cases, the single-exponential decay fitting is sufficient to describe the dwell time description (with A > 0.75, in bold), suggestive of a homogenous population. For the cases where A < 0.75, the double-exponential decay fitting is selected (in bold). For the few cases where the double double-exponential decay fitting is used, the presence of a heterogeneous population is expected:

(1) The dwell time of the 0.5 FRET state of WT T-box/tRNA$^{Ile\text{-}\Delta NCCA}$ complex when analyzing all trajectories is best fit with a double-exponential decay, which is consistent with the presence of two subpopulations: One-state and Two-state populations. The dwell time of 0.5 FRET state in each of the subpopulation is well described with single-exponential decay. Consistent with the presence of two subpopulations in the partially bound state, the dwell time of the 0.4 FRET state in the WT T-box/tRNA^{Ile} and RAG Mutant/tRNA^{Ile} combinations is best described with a double-exponential decay.

(2) The dwell time of the zero FRET state is well described with a single-exponential decay when repetitive tRNA binding is observed, but best described with a double-exponential decay in the cases of WT T-box/tRNA^{Ile} combination, the Two-state subpopulation of WT T-box/tRNA$^{Ile\text{-}\Delta NCCA}$ combination, and RAG Mutant/tRNA^{Ile} combination. In these three cases, the complexes are either already formed before imaging acquisition and/or tRNAs mostly remains bound, therefore the unbound state is incompletely sampled, which can lead to apparent heterogeneity in the population and inaccuracy of dwell time analysis.

Part	Insert sequence
WT *Mtb IleS* T-box	TCTAGATTTTAATACGACTCACTATAGGCATCGATCCGGCGATCACCGGGGAGCCTTC GGAAGAACGGCCGGTTAGGCCCAGTAGAACCGAACGGGTTGGCCCGTCACAGCCTCA AGTCGAGCGGCCGCGCATCGGCGTGGCAAGCGGGGTGGTACCGCGGCGTTCGCGCA CCGGCGTGGCGTCGTCCCCGAAATGTTTGCGGCTGCAGCATTCTTTGCATGC
Linker Mutant	TCTAGATTTTAATACGACTCACTATAGGCATCGATCCGGCGATCACCGGGGAGCCTTC GGAAGAACGGCCGGTTAGGCCCAGTAGAACCGAACGGGTTGGCCCGTCGCACGGCC AAGTCGAGCGGCCGCGCATCGGCGTGGCAAGCGGGGTGGTACCGCGGCGTTCGCGC ACCGGCGTGGCGTCGTCCCCGAAATGTTTGCGGCTGCAGCATTCTTTGCATGC
RAG Sequence Mutant	TCTAGATTTTAATACGACTCACTATAGGCATCGATCCGGCGATCACCGGGGAGCCTTC GGAAGAACGGCCGGTTAGGCCCAGTAGAACCGAACGGGTTGGCCCGTCACAGCCTCA AGTCCGCCGGCCGCGCATCGGCGTGGCAAGCGGGGTGGTACCGCGGCGTTCGCGCA CCGGCGTGGCGTCGTCCCCGAAATGTTTGCGGCTGCAGCATTCTTTGCATGC
Specifier Mutant	TCTAGATTTTAATACGACTCACTATAGGCATCGATCCGGCGTGGACCGGGGAGCCTTC GGAAGAACGGCCGGTTAGGCCCAGTAGAACCGAACGGGTTGGCCCGTCACAGCCTCA AGTCGAGCGGCCGCGCATCGGCGTGGCAAGCGGGGTGGTACCGCGGCGTTCGCGCA CCGGCGTGGCGTCGTCCCCGAAATGTTTGCGGCTGCAGCATTCTTTGCATGC
Δ-Discriminator Mutant	TCTAGATTTTAATACGACTCACTATAGGCATCGATCCGGCGATCACCGGGGAGCCTTC GGAAGAACGGCCGGTTAGGCCCAGTAGAACCGAACGGGTTGGCCCGTCACAGCCTCA AGTCAATGTTTGCGGCTGCAGCATTCTTTGCATGC
Stem II Mutant A	TCTAGATTTTAATACGACTCACTATAGGCATCGATCCGGCGATCACCGGGGAGCCTTA ACCGAACGGGTTGGCCCGTCACAGCCTCAAGTCGAGCGGCCGCGCATCGGCGTGGC AAGCGGGGTGGTACCGCGGCGTTCGCGCACCGGCGTGGCGTCGTCCCCGAAATGTT TGCGGCTGCAGCATTCTTTGCATGC
Stem II Mutant B	TCTAGATTTTAATACGACTCACTATAGGCATCGATCCGGCGATCACCGGGGAGCCTTC GGAAGAAAAGTAGAACCGAACGGGTTGGCCCGTCACAGCCTCAAGTCGAGCGGCCGC GCATCGGCGTGGCAAGCGGGGTGGTACCGCGGCGTTCGCGCACCGGCGTGGCGTCG TCCCCGAAATGTTTGCGGCTGCAGCATTCTTTGCATGC
Stem II Mutant C	TCTAGATTTTAATACGACTCACTATAGGCATCGATCCGGCGATCACCGGGGAGCCTTC GGAAGAACGAAAACAGTAGAACCGAACGGGTTGGCCCGTCACAGCCTCAAGTCGAGC GGCCGCGCATCGGCGTGGCAAGCGGGGTGGTACCGCGGCGTTCGCGCACCGGCGT GGCGTCGTCCCCGAAATGTTTGCGGCTGCAGCATTCTTTGCATGC
IntraFRET	GAATTCTTTTAATACGACTCACTATAGGGGGAAATTAGGGGGGGCATCGATCCGGCGA TCACCGGGGAGCCTTCGGAAGAACGGCCGGTTAGGCCCAGTAGAACCGAACGGGTTG GCCCGTCACAGCCTCAAGTCGAGCGGCCGCGCATCGGCGTGGCAAGCGGGGTGGTA CCGCGGCGTTCGCGCACCGGCGTGGCGTCGTCCCCGAAATGTTTGCGGCTGCTGAG ACCTCTCTCTCTCGGATCC
tRNA^{Ile} WT	TCTAGATTTTAATACGACTCACTATAGGGCCTATAGCTCAGGCGGTTAGAGCGCTTCGC TGATAACGAAGAGGTCGGAGGTTCAAGTCCTCCTAGGCCCACCAAGCATTCTTTGCAT GC
tRNA^{Ile} ΔNCCA	TCTAGATTTTAATACGACTCACTATAGGGCCTATAGCTCAGGCGGTTAGAGCGCTTCGC TGATAACGAAGAGGTCGGAGGTTCAAGTCCTCCTAGGCCCAGCATTCTTTGCATGC
tRNA^{Trp}	TCTAGATTTTAATACGACTCACTATAGGGGGTATAGTTTAATGGTAAAACGAAGGTCTC CAAAACCTTTGATGTGGGTTCGATTCCTACTACCCCCACCAAGCATTCTTTGCATGC
3' Extension Oligo	5'-/Biosg/GCAGCCGCAAACATT/3AmMC6T/-3'

5’ Extension Oligo (for intramolecular experiments)	5’-/AmMC6/CCCCCTAATTTCCCCC-3’

Supplementary Table 7. Sequences used for inserting constructs into cloning vector and for anchoring oligonucleotides.

Part	5' Cloning site	3' Cloning site	Linearization site	T7 Promoter sequence	Overhang for DNA probe annealing (3')	Overhang for DNA probe annealing (5')
WT Mtb IleS T-box	XbaI (TCTAGA)	SphI (GCATGC)	BsmI (GCATTC)	TAATACG ACTCACT ATA	AATGTTTGC GGCTGC	-
Linker Mutant	XbaI (TCTAGA)	SphI (GCATGC)	BsmI (GCATTC)	TAATACG ACTCACT ATA	AATGTTTGC GGCTGC	-
RAG Sequence Mutant	XbaI (TCTAGA)	SphI (GCATGC)	BsmI (GCATTC)	TAATACG ACTCACT ATA	AATGTTTGC GGCTGC	-
Specifier Mutant	XbaI (TCTAGA)	SphI (GCATGC)	BsmI (GCATTC)	TAATACG ACTCACT ATA	AATGTTTGC GGCTGC	-
Δ-Discriminator Mutant	XbaI (TCTAGA)	SphI (GCATGC)	BsmI (GCATTC)	TAATACG ACTCACT ATA	AATGTTTGC GGCTGC	-
Stem II Mutant A	XbaI (TCTAGA)	SphI (GCATGC)	BsmI (GCATTC)	TAATACG ACTCACT ATA	AATGTTTGC GGCTGC	-
Stem II Mutant B	XbaI (TCTAGA)	SphI (GCATGC)	BsmI (GCATTC)	TAATACG ACTCACT ATA	AATGTTTGC GGCTGC	-
Stem II Mutant C	XbaI (TCTAGA)	SphI (GCATGC)	BsmI (GCATTC)	TAATACG ACTCACT ATA	AATGTTTGC GGCTGC	-
IntraFRET	EcoRI (GAATTC)	BamHI (GGATCC)	BsaI (GAGACC)	TAATACG ACTCACT ATA	AATGTTTGC GGCTGC	GGGGGAAA TTAGGGGG
$tRNA^{Ile}$ WT	XbaI (TCTAGA)	SphI (GCATGC)	BsmI (GCATTC)	TAATACG ACTCACT ATA	-	-
$tRNA^{Ile}$ ΔNCCA	XbaI (TCTAGA)	SphI (GCATGC)	BsmI (GCATTC)	TAATACG ACTCACT ATA	-	-
$tRNA^{Trp}$	XbaI (TCTAGA)	SphI (GCATGC)	BsmI (GCATTC)	TAATACG ACTCACT ATA	-	-

Supplementary Table 8. Relevant cloning details.

Supplementary Method

Fitting of biolayer interferometry data

Three binding models were considered to describe the binding kinetics: a one-step binding model, a two-independent binding sites or parallel one-step binding model, and a sequential two-step binding model. In the first model the binding describes one T-box molecule binding to one tRNA molecule following first order kinetics with one association and one dissociation constant (**Supplementary Fig. 1C**). The parallel one-step binding model assumes two independent binding sites in the T-box and a tRNA binding to each site and is described by two sets of association and dissociation constants (**Supplementary Fig. 1C**). Finally, the two-step binding model, described previously in a different context [4], assumes two binding sites between the T-box and the tRNA, and sequential binding to one site (Tbox:$tRNA_1$) followed by binding to the second site (Tbox:$tRNA_2$) (**Supplementary Fig. 1C**). In this model, unbinding also assumes a sequential model but the first step is in only one direction due to the dilution of the tRNA.

The BLI data were fit by the three models using either the Octet Data Analysis Software version 11.1 (FortéBio Inc. San Jose, CA) for the one-step and parallel one-step binding models, or custom written software for the two-step binding model. The one-step and parallel one-step models did not fit the data well (**Supplementary Fig. 2A**), while the two-step binding model produced the best results and described the binding process well (**Supplementary Fig. 2A**). For that reason, all data was subsequently analyzed using the two-step binding model as described below.

In the two-step binding model, the dissociation kinetics were analyzed according to the following scheme:

$$Tbox{:}\,tRNA_2 \underset{k_{-2}}{\overset{k_2}{\rightleftharpoons}} Tbox{:}\,tRNA_1 \underset{k_{-1}}{\overset{}{\rightharpoonup}} Tbox + tRNA \quad (1)$$

Which can be described by the following differential equations:

$$\frac{\partial [Tbox{:}tRNA_1](t)}{\partial t} = k_{-2}\,[Tbox{:}\,tRNA_2] - k_{-1}\,[Tbox{:}\,tRNA_1] - k_2\,[Tbox{:}\,tRNA_1] \quad (2)$$

$$\frac{\partial [Tbox{:}tRNA_2](t)}{\partial t} = k_2\,[Tbox{:}\,tRNA_1] - k_{-2}\,[Tbox{:}\,tRNA_2] \quad (3)$$

The fitted parameters from the dissociation kinetics were then used to fit the following association kinetics according to the following scheme:

$$Tbox + tRNA \underset{k_{-1}}{\overset{k_1}{\rightleftharpoons}} Tbox{:}\,tRNA_1 \underset{k_{-2}}{\overset{k_2}{\rightleftharpoons}} Tbox{:}\,tRNA_2 \quad (4)$$

Which can be described by the following differential equations:

$$\frac{\partial [Tbox{:}tRNA_1](t)}{\partial t} = k_1 \cdot [tRNA] \cdot [Tbox] - [Tbox{:}\,tRNA_1](k_1 \cdot [tRNA] + k_{-1} + k_2) - [Tbox{:}\,tRNA_2](k_1 \cdot [tRNA] - k_{-2}) \quad (5)$$

$$\frac{\partial[Tbox{:}tRNA_2](t)}{\partial t} = k_2\,[Tbox{:}tRNA_1] - k_{-2}\,[Tbox{:}tRNA_2] \quad (6)$$

Association data was fitted by constraining k_1 to be smaller than the diffusion value [4] and the effective concentration of T-box in the biosensors to values previously reported for this type of biosensors [5].

The K_D was calculated according to the formula [4]:

$$K_D = \frac{k_{-1}}{k_1\left(1+\frac{k_2}{k_{-2}}\right)} \quad (7)$$

Python scripts, along with the preprocessed data used to analyze these experiments, are available in the Source Data file.

References

1. Li, S. et al. Structural basis of amino acid surveillance by higher-order tRNA-mRNA interactions. *Nat Struct Mol Biol* **26**, 1094-1105 (2019).
2. Battaglia, R.A., Grigg, J.C. & Ke, A.L. Structural basis for tRNA decoding and aminoacylation sensing by T-box riboregulators. *Nature Structural & Molecular Biology* **26**, 1106-+ (2019).
3. Gruber, A.R., Lorenz, R., Bernhart, S.H., Neubock, R. & Hofacker, I.L. The Vienna RNA websuite. *Nucleic Acids Res* **36**, W70-4 (2008).
4. Schreiber, G., Henis, Y.I. & Sokolovsky, M. Analysis of Ligand-Binding to Receptors by Competition Kinetics - Application to Muscarinic Antagonists in Rat-Brain Cortex. *Journal of Biological Chemistry* **260**, 8789-8794 (1985).
5. Weeramange, C.J., Fairlamb, M.S., Singh, D., Fenton, A.W. & Swint-Kruse, L. The strengths and limitations of using biolayer interferometry to monitor equilibrium titrations of biomolecules. *Protein Science* **29**, 1018-1034 (2020).